ISSN 1027-4510, Journal of Surface Investigation: X-ray, Synchrotron and Neutron Techniques, 2023, Vol. 17, No. 5, pp. 1052–1059. © Pleiades Publishing, Ltd., 2023.
Russian Text © The Author(s), 2023, published in Poverkhnost', 2023, No. 10, pp. 13–21.

Observation of Surface Plasmon Resonance in Monochromatic Terahertz Radiation on Indium Antimonide

I. Sh. Khasanov[a, *], V. V. Gerasimov[b, c, **], O. E. Kameshkov[b, c], A. K. Nikitin[a], and V. V. Kassandrov[d]

[a] *Scientific and Technological Center of Unique Instrumentation, Russian Academy of Sciences, Moscow, 117342 Russia*
[b] *Budker Institute of Nuclear Physics, Siberian Branch, Russian Academy of Sciences, Novosibirsk, 630090 Russia*
[c] *Novosibirsk State University, Novosibirsk, 630090 Russia*
[d] *Peoples' Friendship University of Russia, Moscow, 117198 Russia*
**e-mail: khasanov@ntcup.ru*
***e-mail: v.v.gerasimov3@gmail.com*

Received December 29, 2022; revised February 5, 2023; accepted February 5, 2023

Abstract—Currently, the terahertz-frequency range, which is on the border of the microwave and optical ranges, is being intensively utilized. One of the widely used materials in terahertz optics is indium antimonide (InSb), the plasma frequency of which depends on the degree of doping, temperature, and surface illumination. The possibility of generating surface plasmon polaritons, a type of surface electromagnetic waves, on the surface of an InSb sample using the attenuated-total-reflection method (ATR) (Otto scheme) is discussed. Using the scattering-matrix formalism, the conditions for the highest efficiency of the excitation of surface plasmon polaritons are established. If terahertz radiation with a frequency ω slightly less than ω_p is used for this, the propagation length of such plasmons and the depth of their field penetration into the environment (air) are comparable to the radiation wavelength. It is possible to achieve surface plasmon resonance in the form of a sharp decrease in the intensity of monochromatic radiation reflected from the base of the ATR prism with a change in the angle of incidence and the size of the air gap. Test experiments were performed to observe the surface plasmon resonance on an InSb wafer using a high-resistance silicon prism and monochromatic radiation ($\lambda = 141$ μm) from the Novosibirsk free electron laser. The dependence of the resonant dip on the size of the air gap separating the prism from the sample surface is studied, and its optimal (in the case of resonance) value is established for semiconductors with a plasma frequency in the terahertz range.

Keywords: terahertz radiation, surface plasmon polaritons, indium antimonide, surface electromagnetic waves, surface plasmon resonance, attenuated-total-reflection method, free electron laser

DOI: 10.1134/S1027451023050208

INTRODUCTION

The surface plasmon resonance (SPR) phenomenon makes it possible to concentrate the electromagnetic field energy at sub-wavelength distances ($\delta \ll \lambda$) near a conducting surface, which substantially increases the efficiency of the interaction of light with substances. This effect is the basis of plasmonics, which is a promising area for studies directed on the miniaturization of optical devices for the control, generation, and recording of light at scales smaller than the wavelength of light. Plasmonics techniques are very efficient for designing highly sensitive sensors [1, 2], miniature laser sources [3], and high-speed light modulators [4] for obtaining super-resolution imaging [5]. Plasmonics has proven itself in such applied fields as telecommunications [6] and medicine, including, for example, the problems of detecting viruses [7] and pathogens in food products [8], and determination of the glucose concentration [9]. However, a great part of the studies on plasmonics belongs to the optical range, since traditional plasmon materials (noble metals) do not allow the excitation of surface plasmons with a short propagation length, because their plasma frequency belongs to the short-wavelength spectral region. The extending (extrapolation) of plasmonics methods to the terahertz (THz) range can increase the quality of the results, which were obtained before in the THz range by reflectometry: in particular, the possibility of identifying complex biomolecules [10] and medicine applications for detecting cancer cells [11]. One of the possibilities of this is the use of narrow-gap semiconductors [12], the plasma frequency of which is in the THz spectral range.

One of the most promising semiconductors is indium antimonide (InSb) [13]. In addition, the possibility of doping semiconductors with impurities gives the possibility of controlling the optical response of the surface and optimizing plasmon sensors [14, 15] using heterostructures.

MODELING

SPR in Indium Antimonide

The SPR phenomenon is the excitation of a surface electromagnetic wave at a conducting material–insulator interface. The electric-field strength of a surface electromagnetic wave increases exponentially as the surface directing the wave is approached. This property allows one to attain a high SPR sensitivity to changes in the optical properties of both the surface and also its coatings. Each conducting material has its own resonance frequency above which no resonance is observed and that at which it is most intense. It depends on the plasma frequency ω_p of a material. In the optical range, plasmon materials are metals. However, in the THz range, surface electromagnetic waves on metals are weakly localized [16]; thus, semiconductors are more promising materials for the observation of SPR. In particular, the resonant frequencies of narrow-gap semiconducting III–V compounds are in the THz range [17]. The most promising materials for THz plasmatronics is InSb due to the least effective mass $m^* \approx 0.014m_e$ among Group III–V semiconductors. Thus, InSb has a very high electron mobility. Indium antimonide is a well-studied semiconductor, impurity-free crystals of which can be grown with quite high purity [18] up to 99.9999%. In doped semiconductors (having various concentrations of *p*- and *n*-type charge carriers), uncompensated charge carriers (so-called surface plasmon polaritons [19]) give a contribution to the charge wave on the sample surface conjugate to the surface electromagnetic wave [19]. In the case of plasmon–polariton generation using prisms (the Kretschmann–Raether scheme [20] or the Otto scheme [21] which is more preferable in the THz range [22]), the oscillations of surface electromagnetic waves in uncompensated charge carriers amplify in a resonant way with the equality (proximity) of the wave vector of surface plasmon polaritons (SPP) k_X^{SPP} and the tangential component of the radiation k_X, incident on the prism base at an angle of $\theta > \arcsin(1/n_1)$, which is higher than the critical angle θ_{crit} of the prism material. The radiation energy is transformed to the energy of surface electromagnetic waves, which is observed as an abrupt decrease in the reflected radiation intensity (as a resonant dip) upon angular or frequency scanning of the incident radiation. The angular (frequency) resonance dip width is proportional to the damping of surface plasmon polaritons, which is very sensitive to the surface state [23] and its transition layer, and the closer the radiation frequency ω to the plasma frequency ω_p of the sample material, the higher the sensitivity. If the surface electromagnetic-wave propagation length L (the distance, at which the wave intensity decreases by a factor of $e \approx 2.718$) significantly exceeds the wavelength λ, the resonant dip shape is distorted due to the re-emission of surface electromagnetic waves into the prism within the incident-radiation beam and also beyond it. In the case of metals, values of ω_p belong mainly to near ultraviolet; thus, for metals, L is comparable to λ only in the optical range, where they are used for the observation of SPR due to high localization. In the case of semiconductors, the values of ω_p belong mainly to the THz range (the frequency from 1 to 10 THz), which opens up the possibility of observing and using the SPR phenomena at the surface of such semiconductors and their compounds. Various levels of doping allow us to control the plasma frequency ω_p. For example, an increase in the free-carrier concentration N shifts the plasma frequency $\omega_p = \sqrt{\frac{Ne^2}{\varepsilon_0 m^*}}$ to the short-wavelength range. This fact makes it possible to determine the carrier concentration N according to the optical spectrum. The electric methods of measuring N often give results different from those obtained by optical methods [24]. This is related to the fact that radiative (optical) methods are more sensitive to regions localized on the surface and less sensitive to the carrier concentrations in the semiconductor depth, since the penetration depth of the electromagnetic field of incident radiation is some orders less than the skin-layer depth for the current in the case of electrical measurements.

The optical properties of the semiconductor surface are known to differ from the bulk properties due to the existence of oxides on the surface [25]. Knowledge of the complex permeability at various doping levels allows us to choose the optimum parameters when designing heterostructures. In [26], we assumed that the Otto scheme is promising for the nondestructive testing of semiconductor surfaces, and they can be substrates for SPR microscopy in the THz range [27].

Previously terahertz electromagnetic waves were excited on semiconductor surfaces using a time-domain THz spectroscopy setup [28]. The Otto scheme was used in the THz range to study other narrow-gap semiconductors, for example, indium arsenide (InAs) [29], or semimetals such as silicon [30]. In this work, we used the monochromatic radiation of a free-electron THz laser.

The Drude and Drude–Lorentz models for describing the optical properties of InSb almost coincide at low frequencies of the THz range $\omega < \omega_L/\sqrt{2}$ (ω_L = 179.5 cm^{-1} [17]), i.e., at frequencies of $\omega <$ 127 cm^{-1}. The Lorentz frequency ω_L corresponds to an absorption maximum at the phonon eigenfrequencies of the crystal lattice. Thus, in the THz spectral range, the complex permeability of indium antimon-

ide can be described with good approximation by the Drude model:

$$\varepsilon(\omega) = \varepsilon_\infty - \frac{\omega_p^2}{\omega^2 + \omega_\tau^2} + j\frac{\omega_p^2\omega_\tau}{\omega(\omega^2 + \omega_\tau^2)}. \quad (1)$$

In publications, there are known optical constants in the THz range for pure InSb measured by reflectometric methods. We present the indium antimonide parameters, separating out the parameters used in our numerical analysis by boldface: $\in_\infty$ = 15.4 [31], 15.6 [32], **15.68** [17, 33, 34], 15.7 [35], 15.75 [36]; ω_τ = 3.3 [37], 8.6 [31], 9.6 [33], **10.3** [17], 10.7 cm^{-1} [34]; ω_p = 244.2 [37], 292.2 [33], 296 [31], **302.4** [17], 320.7 cm^{-1} [34]; $N = 6 \times 10^{15}$ cm^{-1} (at low T) [34], 10^{16} cm^{-1} (at room temperature) [35, 38], 3.8×10^{15} cm^{-1} [32], 5×10^{17} cm^{-1} (upon external illumination) [37]; $\mu_e\left(10^4 \frac{\text{cm}^2}{\text{V s}}\right)$ = 6.66 [33, 39], 7.6 [37, 38], 7.7 [35], 9 [32]; $\frac{m^*}{m_e}$ = 0.014 [32, 35], 0.0169 [40].

The concentrations N measured for InSb lie within quite wide limits, which is likely to be related to the different degrees of purity of the samples used, the various treatments of their surfaces [41], and also different temperatures, at which the concentration was measured. For example, the empirical temperature dependence of the carrier concentration in indium antimonide is known [42]: $N = 5.76 \times 10^{14} T^{1.5} \exp\left(-\frac{0.129}{kT}\right)$ cm^{-1}. Thanks to the temperature dependence, indium antimonide is used as the base of hot-electron detectors [43]. It has a high magnetic susceptibility, which allows one to use it in Hall probes. The susceptibility of InSb is used for the magnetic modulation of plasmons in magnetoplasmonics [44]. The high sensitivity of indium antimonide to temperature, the magnetic-field strength, and the illuminance, on the one hand, requires strict monitoring of the sample state and, on the other hand, opens up the possibility of using modulation schemes of measurements, which allows one to attain a high signal-to-noise ratio.

For the collision frequency $\omega_\tau = \frac{m^*\mu_e}{e}$, there are known dependences of the electron mobility μ_e on the carrier concentration N [39]. The effective mass m^* of InSb also has a nonlinear dependence on the carrier concentration [45]: $m^*(N) = m^*\left(1 + \frac{1}{2}\frac{3}{\pi}^{2/3} \frac{h^2}{E_g m^*} N^{2/3}\right)$, where $E_g \approx 0.17$ eV at 300 K. Based on the foregoing, it seems possible to estimate the electronic properties N, μ_e, and m^* of indium antimonide by the frequencies ω_p and ω_τ, which, in turn, can be determined from the optical spectrum $\varepsilon(\omega)$ (1).

Calculation of the Optimum Parameters for the Observation of Resonance on Indium Antimonide

To find the optical constants $\varepsilon(\omega)$ from measurements of the reflectance R, we use the transfer-matrix formalism to calculate electromagnetic-wave propagation through layered media [46]. This method is based on Fresnel equations written using S-matrices. We choose the S-matrix in the form:

$$S = \prod_{i=1}^{N} \begin{bmatrix} \frac{\exp(-jk_{Zi}d_i)}{1-r_i} & \frac{r_i\exp(-jk_{Zi}d_i)}{1-r_i} \\ \frac{r_i\exp(-jk_{Zi}d_i)}{1-r_i} & \frac{\exp(-jk_{Zi}d_i)}{1-r_i} \end{bmatrix}, \quad (2)$$

where i is the number of layers (for the Otto scheme: (*1*) prism, (*2*) air gap, (*3*) semiconductor, j is the complex unit, and d_i is the layer thickness; the wave vector in the ith layer can be determined as $k_i^2 = k_X^2 + k_{Zi}^2$, where k_X is the tangential component, $k_{Zi} = k_0\sqrt{\varepsilon_i - \varepsilon_1\sin(\theta)^2}$ is the normal component, and the complex reflection coefficient at the layer boundaries $r_i = r_{i,i+1}$ are:

$$r_{i,i+1} = \frac{\varepsilon_{i+1}k_{Zi} - \varepsilon_i k_{Zi+1}}{\varepsilon_{i+1}k_{Zi} + \varepsilon_i k_{Zi+1}}. \quad (3)$$

It follows that the reflection coefficient can be found as $R = \left|\frac{S_{21}}{S_{11}}\right|^2 = |r|^2$.

The plasmon resonance is observed if a pole forms in the complex-valued S-matrix. In this case, analytical consideration is hampered; thus, the task of detecting the poles is usually resolved numerically. A detailed analysis for the Otto scheme is given in [21]. The complex reflection coefficient can be written as

$$R_{123} = \left|\frac{r_{12} + r_{23}\exp(2jk_{Z2}d)}{1 + r_{12}r_{23}\exp(2jk_{Z2}d)}\right|^2. \quad (4)$$

The expression for the optimum air gap $d(\varepsilon_2 = 1)$ suitable for numerical analysis is [14]:

$$d = -\frac{j}{2k_{Z2}}\ln\left(-\frac{(k_{Z1} - \varepsilon_1 k_{Z2})(\varepsilon_3 k_{Z2} + k_{Z3})}{(\varepsilon_3 k_{Z2} - k_{Z3})(k_{Z1} + \varepsilon_1 k_{Z2})}\right). \quad (5)$$

Since the logarithm argument in Eq. (5) is complex, Eq. (5) is transcendent and has the set of complex solutions $d = d' + jd''$. The physical solution of Eq. (5) can be only the real value of d, which may be unattainable at all values of angle θ and radiation frequency ω. However, if the imaginary part d'' is small, a weak resonance can arise when the minimum reflection coefficient R_{min} is nonzero, i.e., the surface elec-

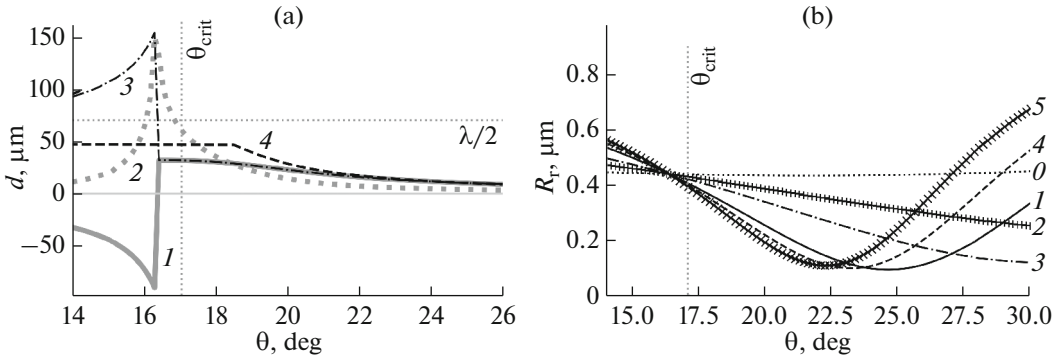

Fig. 1. (a) $d(\theta)$ and (b) $R_r(\theta)$ dependences for InSb at a frequency of $\omega = 71$ cm^{-1} ($\lambda = 141$ μm): (a) diagrams of the (*1*) real d' and (*2*) imaginary d'' parts of the optimum gap value, (*3*) optimum parameters (at which the reflection minimum R_r is observed) d_{min} at (*4*) $\theta = \text{const}$ and θ_{min} at $d = \text{const}$; (b) for various air-gap values with the deviation from the optimal value $d_{SPR} = 11$ μm (*1*) ($\theta_{SPR} = 24°37'$: (*0*) 0, (*2*) 0.25*d*, (*3*) 0.50*d*, (*4*) 1.25 *d*, and (*5*) 1.50 *d*.

tromagnetic wave is excited at these values of the real part of the air gap d', but not effectively ($R_{min} > 0$). We note that the SPR method can be significantly more sensitive than reflectometry but only in the case of the effective excitation of surface electromagnetic waves. As the SPR method is used at suboptimal parameters, the sensitivity of the method can decrease significantly.

From the condition of existing SPR, it follows that the real part $\varepsilon_3' < 0$ must be less than zero. The collision frequency of pure and doped *n*-type InSb is usually much lower than the plasmon frequency $\omega_\tau \ll \omega_p$. Then it can be shown, using the Drude model (1), that SPR takes place only at frequencies $\omega < \omega_p/\sqrt{\varepsilon_\infty}$. For pure InSb, $\dfrac{\omega_p}{\sqrt{\varepsilon_\infty}} = 76.4$ cm^{-1}. In the case of *p*-type InSb, a surface electromagnetic wave is not excited effectively, since the collision frequency ω_τ becomes one order of magnitude higher, i.e., the electrical conductivity of *p*-type InSb is low.

Another important indicator of SPR is observation of the reflection-coefficient minimum at angles larger than the critical angle $\theta > \arcsin(1/\sqrt{\varepsilon_1})$, since it is necessary for the generation of an evanescent wave. If the minima of R are observed at lower angles θ, they are caused by light interference in the air gap and are not related to the initiation of an electromagnetic wave on the semiconductor surface.

We consider the Otto scheme using a prism made of a high-resistance silicon Si ($n = 3.41$) Si ($n = 3.41$) at various frequencies: $\omega < \omega_p/\sqrt{\varepsilon_\infty}$ (63 cm^{-1}), $\omega \approx \omega_p/\sqrt{\varepsilon_\infty}$ (for example, $\omega = 71$ cm^{-1}) and $\omega > \omega_p/\sqrt{\varepsilon_\infty}$ (80 cm^{-1}). We find the optimum parameters for the observation of SPR in the case of InSb by constructing a diagram for $d(\theta)$ and the corresponding resonance curves $R_p(\theta)$ for the optimum parameters d_{SPR} and θ_{SPR} found by the $d(\theta)$ diagram.

From the diagram analysis, it can be concluded that the resonance is not excited effectively near frequencies $\omega \approx \omega_p/\sqrt{\varepsilon_\infty}$ (Fig. 1); i.e., d'' is nonzero at all values of angles θ. However, a weak resonance is observed at some angles $d'' \approx 0$ and $d' \gg d''$, since it is near the *S*-matrix pole. In this case, resonance is excited most effectively at angle θ_{SPR} as plots d_{min} and θ_{min} intersect. At lower frequencies $\omega < \omega_p/\sqrt{\varepsilon_\infty}$ (Fig. 2), as long as the permittivity is low $|\varepsilon(\omega)| \approx 1 - 100$, the resonance can be effectively attained (i.e., $R(\theta_{SPR}) = 0$), when $d''(\theta_{SPR}) = 0$. At high frequencies $\omega > \omega_p/\sqrt{\varepsilon_\infty}$, no plasmon resonance is observed (Fig. 3), since $d' \ll d''$. In this case, the reflection minimum is caused by the absorption of the evanescent wave in the semiconductor substrate above the critical angle θ_{crit}. That is lower values of R_r cannot be obtained as the gap d increases; conversely, the absorption efficiency decreases as the gap increases.

In the plots of the resonance curves, the dot-and-dash line in the case $d = 0$ (i.e., in the case when the prism is in contact with the substrate) demonstrates the absorption of the evanescent wave in the semiconductor bulk; i.e., the measurements are performed in the reflectometry mode. In the case of the observation of SPR (Figs. 1 and 2), the reflection minimum is, as a rule, lower than that in the case of reflectometry and at these observation angles.

To form the concept of accuracy of the SPR method when determining the optical constants of InSb, we calculate them taking into account the measurement error. Most reflectometric setups (including that we designed) operate in the range of incidence angles from 10° to 75°. In the case of reflectometry, the reflection coefficient is calculated as $R_{12} = |r_{12}|^2$.

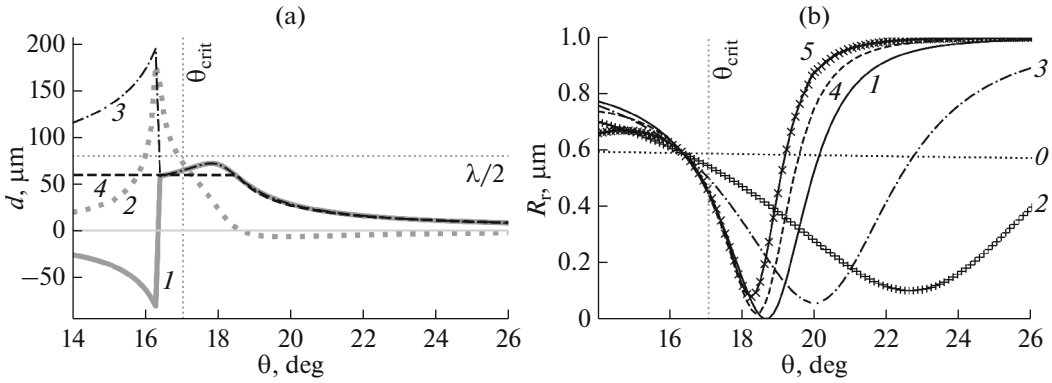

Fig. 2. (a) $d(\theta)$ and (b) $R_r(\theta)$ dependences for InSb at a frequency of $\omega = 63$ cm^{-1} ($\lambda = 159$ μm): (a) diagrams of the (*1*) real d' and (*2*) imaginary d'' parts of the optimum gap value, (*3*) optimum parameters (at which the reflection minimum R_r is observed) d_{min} at (*4*) $\theta = \text{const}$ and θ_{min} at $d = \text{const}$; (b) for various air-gap values with the deviation from the optimal value $d_{SPR} = 54.4$ μm (*1*) ($\theta_{SPR} = 18°39'$: (*0*) 0, (*2*) 0.25*d*, (*3*) 0.50*d*, (*4*) 1.25 *d*, and (*5*) 1.50 *d*.

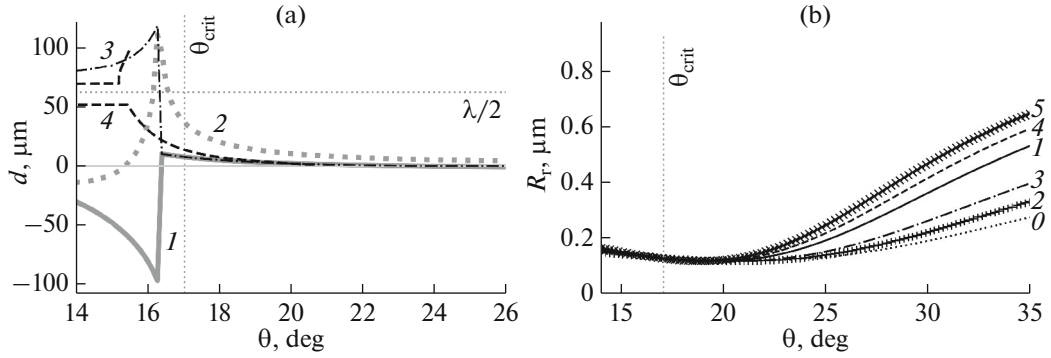

Fig. 3. (a) $d(\theta)$ and (b) $R_r(\theta)$ dependences for InSb at a frequency of $\omega = 80$ cm^{-1} ($\lambda = 125$ μm): (a) diagrams of the (*1*) real d' and (*2*) imaginary d'' parts of the optimum gap value, (*3*) optimum parameters (at which the reflection minimum R_r is observed) d_{min} at (*4*) $\theta = \text{const}$ and θ_{min} at $d = \text{const}$; (b) for various air-gap values $d = 3$ μm (*1*); SPR is not observed: (*0*) 0, (*2*) 0.25*d*, (*3*) 0.50*d*, (*4*) 1.25 *d*, and (*5*) 1.50 *d*.

We take the measurement error of R as 1%, the error of the angle 6′, and the error of the gap 1 μm. Using the Monte Carlo method (i.e., randomizing real values of d, θ, and R, according to the given errors) and the algorithm of reducing the optical constants [47], we find the error in determining the permittivity (Table 1). From Table 1, we can conclude that the accuracies of both the methods are comparable.

However, the SPR method is more sensitive to the value of the permittivity of a surface substance layer. We consider a pure InSb sample into which an *n*-type InSb layer with the thickness $d_4 = 1$ nm is embedded at depth δ. To estimate the method sensitivity, we compare the maximum changes $\max(\Delta R)/\Delta\delta$ caused by displacement of this layer along the depth (Fig. 4). Although the field-penetration depth $1/2k_Z''$ is the same for the optical methods, the field near the surface is more intense in the case of SPR; as a result, this method is almost one order of magnitude more sensitive to impurities in the semiconductor-layer depth.

Table 1. Comparison of the accuracies of the SPR method and reflectrometry when recovering the permittivity ε ($\omega = 63$ cm^{-1})

Parameters	Actual value	SPR	Reflectometry
ε'	−6.83	−6.82 ± 0.07	−6.83 ± 0.08
ε''	3.69	3.68 ± 0.05	3.67 ± 0.05

EXPERIMENTAL

To observe SPR in indium antimonide in the THz range, we assembled an experimental setup based on the Otto scheme (Fig. 5) that makes it possible to perform scanning by the angle and the air-gap width. The Novosibirsk free-electron laser, which is a radiation source tunable in wide range, was used as the monochromatic-radiation source. Previously it was used for works on THz plasmonics using metals as substrates with various dielectric coatings [13, 48–50] for the excitation of an electromagnetic wave on an open waveguide surface. The working frequency was $\lambda = 141$ μm as the most powerful and stable line of THz radiation that is not absorbed by atmospheric water vapor. The THz-radiation power was controlled by filter *1*. To increase the sensitivity of the measurements, the THz radiation was modulated using an optomechanical modulator *2* combined with a Standard Research SR830 synchronous detector. The initial beam 12 mm in diameter was directed by q system of mirrors *3* and limited by diaphragm *4* with a gap of ≈8 mm in diameter; then the beam was narrowed by a factor of four, using telescopic system *6*. A cylindrical prism made of high-resistance silicon Si (*n*) was used as the ATR prism. The THz radiation was polarized in the incident plane on the prism base by polarizer *5*. The reflected radiation was recorded by a Goley cell 7 (Tydex GC-1P) optoacoustic detector. Angular scanning was performed using goniometric table *8*; the positional accuracy was up to 36″. The setup provided a working angular scanning range from 10° to 75°. The scanning according to the air-gap value ($R_{min} > 0$) was carried out using a Standa motorized micromechanical translator *9* that ensures a positional accuracy up to 1 μm. The sample was undoped InSb made by AO Giredmet. The InSb crystal exhibits the electronic type of electrical conductivity, it is oriented in the (100) plane, and has a circular plate form 65 mm in diameter and 1.8 mm in thickness; the roughness is 0.5 μm.

A number of angular scannings were carried out at various fixed distances from the prism base to the substrate, and the reflection minimum was detected at angles higher than the critical prism angle $\theta_{crit} = 17°$ (Fig. 6), which demonstrates the excitation of plasmon polaritons on the indium-antimonide surface.

DISCUSSION

The experimental data shown in Fig. 6 qualitatively demonstrate the behavior of the resonance curve with a change in the air-gap width that corresponds to the expected behavior. The reflection minimum is observed after the critical angle, which is interpreted as SPR. However, the measurements were carried out by the inadequately reliable method of determining the air-gap width: we took the gap value $d = 0$ μm as the contact of the prism surface with the substrate was fixed visually, which can cause an error in giving the

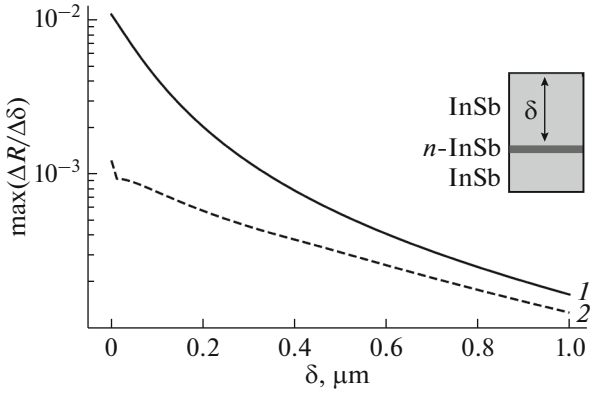

Fig. 4. Sensitivities of (*1*) the SPR method and (*2*) reflectometry over depth at $\omega = 63$ cm^{-1}.

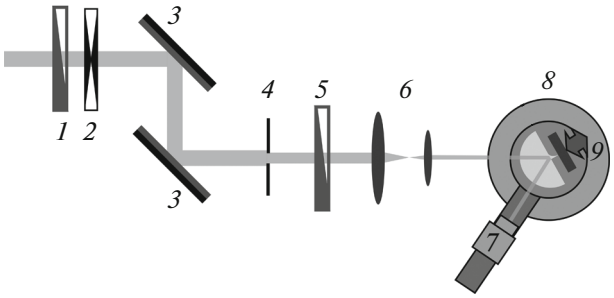

Fig. 5. Setup diagram for the observation of SPR in the THz range: (*1*) filter, (*2*) optomechanical modulator, (*3*) mirror, (*4*), diaphragm, (*5*) polarizer, (*6*) telescopic system, (*7*) detector, (*8*) goniometer, (*9*) translator.

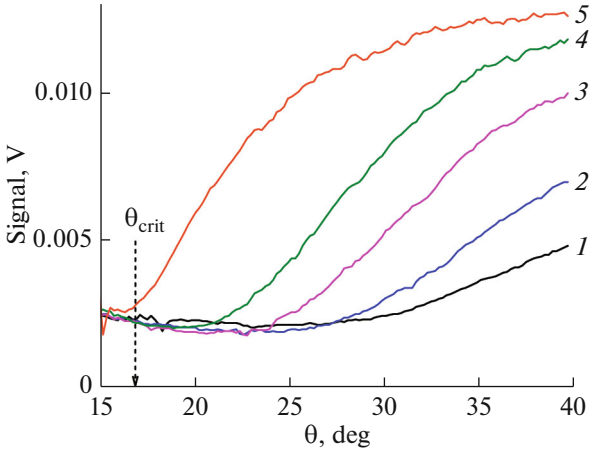

Fig. 6. Dependence of the intensity of *p*-polarized radiation with the wavelength $\lambda = 141$ μm on the incidence angle θ measured for the "silicon prism–air gap of value *d*–InSb plate surface" at *d*: (*1*) 70, (*2*) 100, (*3*) 120, (*4*) 130, and (*5*) 170 μm.

absolute-gap value of several tens of micrometers. Because of this the optical constants of indium antimonide cannot be recovered from the available experimental data. Moreover, for the scheme with a cylindrical prism, it is very important to have a radiation beam thin with respect to the prism sizes to eliminate self-focusing effects. A more appropriate version of the scheme adjustment is the use of prisms with flat faces, for example, a rectangular prism.

Nevertheless, the measurements performed in this work confirm the working efficiency of this assembled experimental scheme and allow us, after eliminating the above drawbacks, to determine the optical constants of indium antimonide and to perform other measurements using the SPR phenomenon. It can be stated that the Otto scheme with terahertz laser radiation is promising for studying semiconductors and also their heterostructures. The SPR method is more sensitive to the surface properties than the reflectometry due to exponential distribution of the energy of a surface electromagnetic wave. The developed method of THz-plasmonics should allow one to measure thin epitaxial layers and to distinguish thin heterostructures near the surface.

CONCLUSIONS

Theoretical and experimental studies showed that surface plasmon resonance can be observed in the THz range on indium antimonide using the Otto scheme and laser radiation. The experimental setup allows us to perform angular scanning and scanning according to the air-gap width, and also tuning of the laser source; these features make it possible to adjust the Otto-scheme parameters to effectively excite SPR in an InSb substrate including InSb doped to high free-carrier concentrations.

ACKNOWLEDGMENTS

This work was performed using equipment of the Collective Use Center "Siberian Center of Synchrotron and Terahertz Radiation" on the base of the universal scientific installation Novosibirsk free-electron laser at the Institute of Nuclear Physics, Siberian Branch, Russian Academy of Sciences.

FUNDING

Theoretical analysis was supported by the Ministry of Science and Higher Education of the Russian Federation (state assignment FFNS-2022-0009) V.K. acknowledges support from Project no. FSSF-2023-0003.

CONFLICT OF INTEREST

The authors declare that they have no conflicts of interest.

REFERENCES

1. M. Soler and L. M. Lechuga, J. Appl. Phys. **129**, 111102 (2021). https://doi.org/10.1063/5.0042811
2. L. C. Oliveira, A. M. Nogueira Lima, C. Thirstrup, and H. F. Neff, *Surface Plasmon Resonance Sensors: A Materials Guide to Design, Characterization, Optimization, and Usage* (Springer, Cham, 2015).
3. P. Berini and I. de Leon, Nat. Photonics **6**, 16 (2012). https://doi.org/10.1038/nphoton.2011.285
4. M. Ayata, Y. Fedoryshyn, W. Heni, B. Baeuerle, A. Josten, M. Zahner, U. Koch, Y. Salamin, C. Hoessbacher, C. Haffner, D. L. Elder, L. R. Dalton, and J. Leuthold, Science **358**, 630 (2017). https://doi.org/10.1126/science.aan5953
5. Z. Liu, *Plasmonics and Super-Resolution Imaging* (Jenny Stanford, New York, 2017).
6. W. O. F. Carvalho and J. R. Mejia-Salazar, Sensors **20**, 2488 (2020). https://doi.org/10.3390/s20092488
7. A. M. Shrivastav, U. Cvelbar, and I. Abdulhalim, Commun. Biol. **4**, 70 (2021). https://doi.org/10.1038/s42003-020-01615-8
8. S. Balbinot, A. M. Srivastav, J. Vidic, I. Abdulhalim, M. Manzano, Trends Food Sci. Technol. **111**, 128 (2021). https://doi.org/10.1016/j.tifs.2021.02.057
9. Q.-H. Phan, Q.-H. Phan, Y.-R. Lai, W.-Z. Xiao, T.-T. Pham, and C.-H. Lien, Opt. Express **28**, 24889 (2020). https://doi.org/10.1364/OE.400721
10. X. Chen, H. Lindley-Hatcher, R. I. Stantchev, J. Wang, K. Li, A. Serrano Hernandez, Z. D. Taylor, E. Castro-Camus, and E. Pickwell-MacPherson, Chem. Phys. Rev. **3**, 011311 (2022). https://doi.org/10.1063/5.0068979
11. A. Banerjee, B. Chakraborty, H. Inokawa, and R. J. Nath, *Terahertz Biomedical and Healthcare Technologies: Materials to Devices* (Elsevier, Amsterdam, 2020).
12. A. Krotkus, J. Phys. D: Appl. Phys. **43**, 273001 (2010). https://doi.org/10.1088/0022-3727/43/27/273001
13. J. S. Ranjana, Investigations on InSb plasmonic devices for sensor applications at terahertz frequencies, PhD Thesis (Surathkal: Natl. Inst. Technol. Karnataka, 2017).
14. D. Barchiesi, in *New Perspectives in Biosensors Technology and Applications*, Ed. by P. A. Serra (IntechOpen, London, 2011), p. 105. https://doi.org/10.5772/16657
15. O. Kameshkov, V. Gerasimov, and B. Knyazev, Sensors **22**, 172 (2021). https://doi.org/10.3390/s22010172
16. V. V. Gerasimov, B. A. Knyazev, I. A. Kotelnikov, A. K. Nikitin, V. S. Cherkassky, G. N. Kulipanov, and G. N. Zhizhin, J. Opt. Soc. Am. B **30**, 2182 (2013). https://doi.org/10.1364/JOSAB.30.002182
17. J. Chochol, K. Postava, M. Čada, M. Vanwolleghem, M. Mičica, L. Halagačka, J.-F. Lampin, and J. Pištora, J. Eur. Opt. Soc.-Rapid Publ **13**, 13 (2017). https://doi.org/10.1186/s41476-017-0044-x

18. *Handbook Series on Semiconductor Parameters*, Vol. 1: *Si, Ge, C (Diamond), GaAs, GaP, GaSb, InAs, InP, InSb*, Ed. by M. Levinshtein, S. Rumyantsev, and M. Shur, (World Sci., Singapore, 2000).

19. *Surface Polaritons: Electromagnetic Waves at Surfaces and Interfaces*, Ed. by V. M. Agranovich and D. L. Mills (Elsevier, New York, 1982; Nauka, Moscow, 1985).

20. H. Raether, *Surface Plasmons on Smooth and Rough Surfaces and on Gratings* (Springer, Heidelberg, 1988). https://doi.org/10.1007/BFb0048319

21. D. Barchiesi and A. Otto, Riv. Nuovo Cimento **36**, 173 (2013). https://doi.org/10.1393/ncr/i2013-10088-9

22. J. Shibayama, K. Mitsutake, J. Yamauchi, and H. Nakano, Microwave Opt. Technol. Lett. **63**, 103 (2021). https://doi.org/10.1002/mop.32581

23. M. M. Nazarov, E. A. Bezus, and A. P. Shkurinov, Laser Phys. **23**, 056008 (2013).

24. M. Hilal, B. Rashid, S. H. Khan, and A. Khan, Mater. Chem. Phys. **184**, 41 (2016). https://doi.org/10.1016/j.matchemphys.2016.09.009

25. O. S. Komkov, D. D. Firsov, T. V. Lvova, I. V. Sedova, A. N. Semenov, V. A. Solov'ev, and S. V. Ivanov, Phys. Solid State **58**, 2394 (2016).

26. A. K. Nikitin, V. V. Gerasimov, B. A. Knyazev, N. T. H. Lien, and T. T. Trang, J. Phys.: Conf. Ser. **1636**, 012036 (2020). https://doi.org/10.1088/1742-6596/1636/1/012036

27. I. Sh. Khasanov, L. A. Zykova, A. K. Nikitin, B. A. Knyazev, V. V. Gerasimov, and T. T. Trang, in *Proc. 45th Int. Conf. on Infrared, Millimeter, and Terahertz Waves* (Buffalo, 2020), p. 1. https://doi.org/10.1109/IRMMW-THz46771.2020.9370795

28. J. Chochol, M. Mičica, K. Postava, M. Vanwolleghem, J.-F. Lampin, M. Čada, and J. Pištora, in Proc. 43rd Int. Conf. on Infrared, Millimeter, and Terahertz Waves (Nagoya, 2018), p. 1. https://doi.org/10.1109/IRMMW-THz.2018.8510484

29. H. Hirori, M. Nagai, and K. Tanaka, Opt. Express **13**, 10801 (2005). https://doi.org/10.1364/OPEX.13.010801

30. M. M. Nazarov, A. P. Shkurinov, F. Garet, and J.-L. Coutaz, IEEE Trans. Terahertz Sci. Technol. **5**, 680 (2015). https://doi.org/10.1109/TTHZ.2015.2443562

31. K. Postava, J. Chochol, M. Mičica, M. Vanwolleghem, P. Kolejak, L. Halagačka, M. Čada, J. Pištora, and J.-F. Lampin, Proc. SPIE **10142**, 1014207 (2016). https://doi.org/10.1117/12.2264550

32. S. C. Howells and L. A. Schlie, Appl. Phys. Lett. **69**, 550 (1996). https://doi.org/10.1063/1.117783

33. J. Chochol, K. Postava, M. Čada, M. Vanwolleghem, L. Halagačka, J.-F. Lampin, and J. Pištora, AIP Adv **6**, 115021 (2016). https://doi.org/10.1063/1.4968178

34. E. Palik, *Handbook of Optical Constants of Solids* (Academic, New York, 1991).

35. Q. Wang, Q. Tang, D. Zhang, Z. Wang, and Y. Huang, Superlattices Microstruct. **75**, 955 (2014). https://doi.org/10.1016/j.spmi.2014.09.015

36. J. Tao, B. Hu, X. Y. He, and Q. J. Wang, IEEE Trans. Nanotechnol. **12**, 1191 (2013). https://doi.org/10.1109/TNANO.2013.2285127

37. T. H. Isaac, J. Gómez Rivas, J. R. Sambles, W. L. Barnes, and E. Hendry, Phys. Rev. B **77**, 113411 (2008). https://doi.org/10.1103/PhysRevB.77.113411

38. P. Gu, M. Tani, S. Kono, K. Sakai, and X.-C. Zhang, J. Appl. Phys. **91**, 5533 (2002). https://doi.org/10.1063/1.1465507

39. E. Litwin-Staszewska, W. Szymanska, and R. Piotrzkowski, Phys. Status Solidi B **106**, 551 (1981). https://doi.org/10.1002/pssb.2221060217

40. J. Chochol, K. Postava, M. Čada, and J. Pištora, Sci. Rep. **7**, 13117 (2017). https://doi.org/10.1038/s41598-017-13394-0

41. T. V. Lvova, M. S. Dunaevskii, M. V. Lebedev, A. L. Shakhmin, I. V. Sedova, and S. V. Ivanov, Semiconductors **47**, 721 (2013).

42. R. W. Cunningham and J. B. Gruber, J. Appl. Phys. **41**, 1804 (1970). https://doi.org/10.1063/1.1659107

43. E. H. Putley, Appl. Opt. **4**, 649 (1965). https://doi.org/10.1364/AO.4.000649

44. F. Fan, S. Chen, and S.-J. Chang, IEEE J. Sel. Top. Quantum Electron. **23**, 8500111 (2017). https://doi.org/10.1109/JSTQE.2016.2537259

45. P. Byszewski, J. Kolodziejczak, and S. Zukotynski, Phys. Status Solidi B **3**, 1880 (1963). https://doi.org/10.1002/pssb.19630031014

46. S. J. Byrnes, arXiv:1603.02720[physics] (2020).

47. A. V. Anisimov and I. Sh. Khasanov, J. Phys.: Conf. Ser. **2091**, 012067 (2021). https://doi.org/10.1088/1742-6596/2091/1/012067

48. V. V. Gerasimov, J. Opt. Technol. **77**, 465 (2010). https://doi.org/10.1364/JOT.77.000465

49. V. V. Gerasimov, G. N. Zhizhin, B. A. Knyazev, I. A. Kotelnikov, N. A. Mitina, and A. K. Nikitin, Bull. Russ. Acad Sci.: Phys. **77**, 1167 (2013). https://doi.org/10.3103/S1062873813090141

50. B. A. Knyazev, AIP Conf. Proc. **2299**, 030001 (2020). https://doi.org/10.1063/5.0030349

Translated by Yu. Ryzhkov